

We are IntechOpen, the world's leading publisher of Open Access books Built by scientists, for scientists

6,900

Open access books available

186,000

International authors and editors

200M

Downloads

Our authors are among the

154

Countries delivered to

TOP 1%

most cited scientists

12.2%

Contributors from top 500 universities



WEB OF SCIENCE™

Selection of our books indexed in the Book Citation Index
in Web of Science™ Core Collection (BKCI)

Interested in publishing with us?
Contact book.department@intechopen.com

Numbers displayed above are based on latest data collected.
For more information visit www.intechopen.com



Nanowires on a Film for Photoelectrochemical Water Splitting

Miao Zhong, Mario Kurniawan,
Aleksandra Apostoluk, Bertrand Vilquin and
Jean-Jacques Delaunay

Additional information is available at the end of the chapter

<http://dx.doi.org/10.5772/52593>

1. Introduction

Nanowires-on-a-film structure (NFS) consisting of a dense array of semiconductor nanowires on a conductive film has recently attracted much interest due to their wide range of applications in electronic, optoelectronic, electromechanic and electrochemical devices [15, 5, 25]. Thanks to their 3D geometry, NFSs provide various morphology-induced advantages resulting in improved devices performances. In addition, as the array of semiconductor NFSs can be grown on a conductive film, which realizes electrical connection between the nanowires, the integration of this nanostructured layer into devices is greatly facilitated.

In this chapter, we review the applications of NFSs as efficient photoanodes in photoelectrochemical (PEC) water splitting cells. Recently, the efficiency of the PEC cells has been reported to be enhanced with the use of semiconductor NFSs [23, 10, 30, 32]. The well-aligned geometry of a nanowire array serves as an anti-reflector in order to enhance light absorption in the structure. Also, an effective separation of the photo-generated carriers is achieved along the transverse direction of the nanowires due to the drastically reduced transport distance of minority carriers. Furthermore, the nanowire array possesses large surface areas that greatly enhance the chemical reaction of water splitting as compared to its smooth film counterpart. Lastly, the underneath film realizes electrical connection between the top nanowires. As a consequence, the semiconductor NFS offers a great potential for PEC water splitting applications. However, the fabrication of high quality NFS with functional semiconductor materials still remains a challenge. Single crystalline functional semiconduc-

tor materials will ensure the photoanodes to have adequate semiconducting and electrochemical properties, leading to fulfill the PEC water splitting requirements [14, 2], including:

- Efficient light absorption
- Effective carrier separation and transport
- Suitable energy band position for redox reaction of water
- Anti-photocorrosive property in the presence of water.

Furthermore, a controllable approach for the fabrication of the NFSs that enables production of large-area photoanodes at a low cost is not far from being achieved [34].

In the following sections, emphases are placed on the synthesis, property and PEC performance of the NFSs fabricated using various materials. The materials under review include TiO_2 , Fe_2O_3 and ZnO , as they have the potential to achieve good performance in PEC water splitting. In addition, surface coating of the ZnO NFS with anti-photocorrosive ZnGa_2O_4 photocatalyst layer is discussed as a mean to improve the stability of the ZnO based photoanodes. Finally, the remaining challenges for the NFS to be used as efficient photoelectrodes for PEC water splitting are presented. It should be noted that the NFS described here are based on arrays of one-dimensional (1D) nanowires, however, nanostructured photoanodes based on nanotubes, nanoplates and other nanostructures on a film should also provide improved PEC device performance.

2. TiO_2 NFSs for PEC water splitting

Since the phenomenon of water electrolysis on a titanium dioxide (TiO_2) electrode under UV light illumination was discovered by [9], TiO_2 has been considered as one of the most promising photocatalysts for energy conversion applications. Later in 1977, Frank and Bard achieved the decomposition of cyanide in water using TiO_2 material under UV light illumination [7]. This achievement further confirmed the photocatalytic behavior of TiO_2 material and led to the use of TiO_2 in environmental and pollution-degradation applications. Recently, extensive research has been conducted on the TiO_2 nanostructures in order to enhance device performances [3]. Versatile morphologies including TiO_2 nanowires, nanosheets, and nanotubes have been fabricated through different chemical and physical approaches. In many reports, the vertical alignment of the TiO_2 nano-architectures perpendicular to the substrates is found to be a crucial factor necessary to improve device performances [8, 10]. In this section, we focus on the synthesis, characterizations and PEC performances of TiO_2 NFSs.

2.1. Synthesis of the TiO₂ NFSs

Titanium (Ti) is a relatively refractory metal with a high melting temperature of about 1670 °C under air condition. This high melting temperature results in a low Ti vapor pressure of $\sim 10^{-3}$ Torr at 1577 °C, which hinders the TiO₂ nucleation in the direct Ti vapor-phase deposition processes such as the physical vapor deposition (PVD) and the thermal chemical vapor deposition (CVD). In order to increase the Ti precursor concentration for the growth of 1D TiO₂ nanostructures, hydrothermal growth, sol-gel growth and metal organic chemical vapor deposition (MOCVD) using Ti organic compounds as precursors are often employed [3].

The fabrication of TiO₂ NFS via the hydrothermal growth method has been proved to be efficient due to its low-temperature processing (which helps to protect the bottom conductive film during the growth of 1D nanowires), mass production of the nanowires, and their easily controllable alignment. As reported by [10], a densely packed, vertically aligned and single crystalline TiO₂ rutile nanowire array was synthesized on a transparent conductive layer consisting of fluorine-doped tin oxide (FTO) via the hydrothermal method. The fabrication process is described in the following.

The FTO coated glass substrate was first cleaned by sonication in a mixture of ethanol and water for 30 minutes in order to remove the impurities on the surface of the substrate. Then, a seed layer of TiO₂ was synthesized on the cleaned FTO coated glass substrate by a first-step hydrothermal growth. The FTO substrate was soaked in a 0.025 M TiCl₄ with n-hexane solution for 30 minutes. The sample was then rinsed with ethanol and finally annealed at 500°C for 30 minutes in air to form a thin layer of TiO₂ on the surface of the substrate. The formation of the TiO₂-seeded layer on the FTO substrate improved the control and the integrity of the later TiO₂ nanowires growth. Moreover, the TiO₂-seeded layer on the FTO layer prevented the formation of electrical short circuits between the electrode and the electrolyte when used as photoanode in the PEC water splitting cell, which guaranteed the photocatalytic function of the TiO₂ photoanode. In the next fabrication step, the TiO₂ nanowires were grown on the TiO₂-seeded FTO substrate with a typical hydrothermal growth procedure. The seeded FTO substrate was placed in sealed Teflon-lined autoclave containing 50 mL of n-hexane, 5 mL of HCL and 2.5-5 mL of titanium isopropoxide. After the reaction was performed at 150°C for a certain amount of time, the autoclave was cooled down to room temperature and finally the TiO₂ NFS was synthesized.

2.2. Characterization of the TiO₂ NFSs

Cross-sectional and top view scanning electron microscope (SEM) images of the synthesized TiO₂ nanowires array are shown in Fig. 1 a and 1b [10]. The TiO₂ nanowires array consisting of vertically aligned and tetragonal shaped nanowires is highly uniform and densely packed on the FTO coated glass substrate. The average diameter of the nanowires is ~ 5 nm and their length is up to ~ 4.5 μm . The length of the nanowires can be tuned from ~ 0.5 to ~ 5 μm , by modifying the synthesis conditions including the precursors ratio (titanium isopropoxide/n-hexane), the reaction time and the thickness of TiO₂ seed layer. [10]

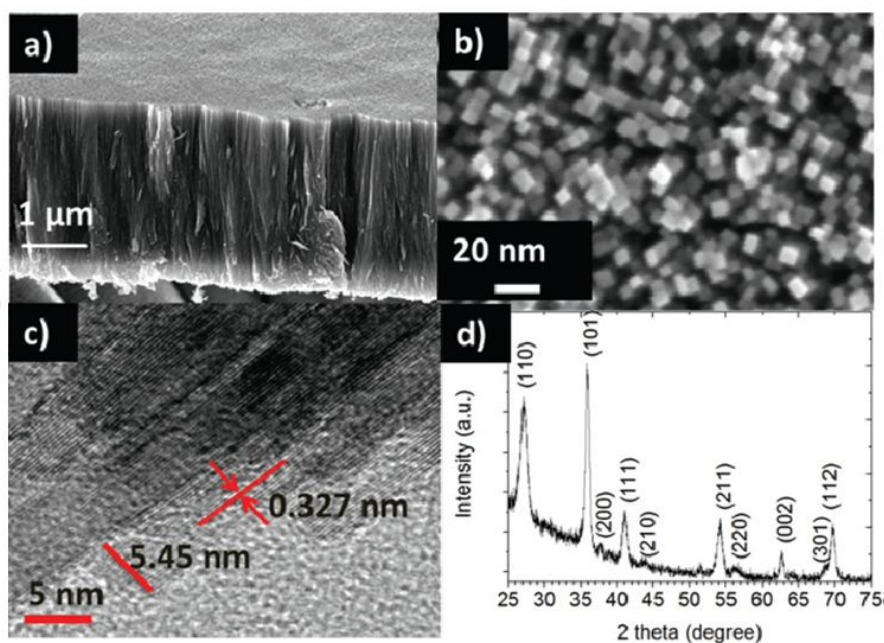


Figure 1. Vertically aligned rutile TiO_2 nanowires. (a) Cross-sectional SEM image, (b) top view SEM image, (c) HRTEM image and (d) GIXRD pattern. Reprinted with permission from [Son 10]. Copyright © 2012, American Chemical Society.

The synthesized TiO_2 nanowires array was characterized by grazing incidence angle X-ray diffraction (GIXRD) technique as shown in Fig. 1 d. The TiO_2 nanowires structure was identified as a rutile crystal from the reference XRD data measured with standard rutile TiO_2 powder. Furthermore, the high resolution transmission electron (HRTEM) image in Fig. 1d showed that the observed rutile phase TiO_2 nanowire is of a single crystal quality, having clear (110) lattice fringes.

2.3. PEC performance of the TiO_2 NFSs

The PEC performance of the synthesized TiO_2 NFS (as previously described) was examined in a three-electrode PEC water splitting cell [10]. The TiO_2 NFS was used as the working electrode, a saturated Ag/AgCl electrode as the reference electrode and a platinum wire as the counter electrode. The electrolyte consisted of one mol/liter KOH solution with pH = 13.5. For the PEC test, TiO_2 nanowires with an average diameter of ~5 nm and average length of ~1.5 μm [10] were studied. The linear sweep voltammetry measurement was performed under a 100 W Xenon lamp illumination ($300 \text{ nm} < \text{wavelength } \lambda < 800 \text{ nm}$) with a bias swept from -0.8 to 0.6 V (vs. Ag/AgCl), as shown in Fig. 2 a. A photocurrent density of ~0.35 mA/cm^2 was obtained at a bias of 1.23 V_{RHE} [10].

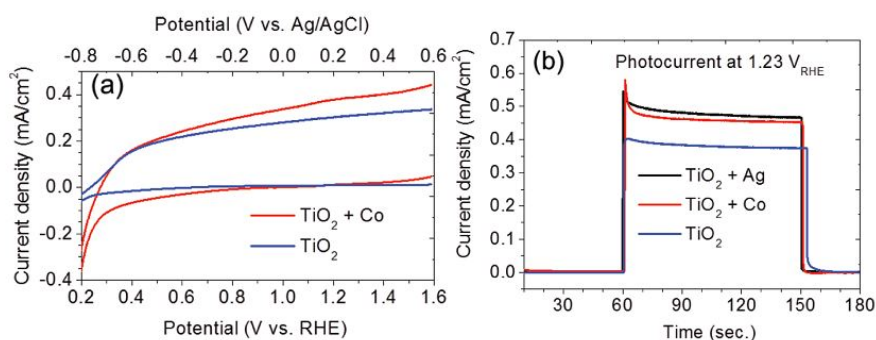


Figure 2. a) Linear sweep voltammetry measurements of the TiO₂ NFS with and without Co treatment, (b) Chronoamperometry measurements of the TiO₂ NFS, Co treated TiO₂ NFS and Ag treated TiO₂ NFS at 1.23 V_{RHE}. Reprinted with permission from [Son 10]. Copyright © 2012, American Chemical Society.

As reported by Tilley et al. [23, 10], decoration of a photoelectrode with metal nanoparticles as co-catalysts exhibited an enhanced yield in hydrogen generation. [10], reported treatments by cobalt (Co) and silver (Ag) performed on the TiO₂ NFS samples. The photocurrent density of ~0.35 mA/cm² measured on the undoped TiO₂ NFS increased to ~0.45 mA/cm² for the Co and Ag coated TiO₂ NFSs, as shown in Fig. 2 b. The enhancement of the photocurrent after Co and Ag treatments was likely related to the improvement in the extraction of photo-generated holes from the surface of the TiO₂ NFS to the electrolyte, through the Co and Ag nanoparticles [23, 10].

3. Hematite NFS for PEC water splitting

Hematite (α -Fe₂O₃ or iron oxide) has been widely investigated as a photocatalyst candidate for PEC water splitting [13, 14, 30] because of its abundance on Earth, its non-toxicity to environment and its stability in water under light illumination. In addition, a band gap between 2.1 and 2.2 eV of the hematite enables visible light absorption and thus makes this material promising for water splitting under solar light illumination. However, hematite has also some disadvantages such as: small light absorption coefficient, short lifetime of the excited-state carrier (10⁻¹² s), short hole diffusion length (2-4 nm), inefficient oxygen evolution reaction kinetics and improper position of the conduction band for hydrogen generation [23, 16], limiting the hematite PEC performance. Different research groups made many efforts to address these issues [23, 14, 16, 10]. To date, improved performances have been realized in the following areas:

1. the synthesis of hematite nanostructures to increase the surface areas;
2. the modification of its electronic structure via elemental doping [23, 14, 16, 10] to enhance the conductivity;
3. the surface decoration with other co-catalysts to reduce the onset water splitting potential.

In the following section, we summarized the results obtained with the silicon-doped hematite nanowire-like array on a conductive film structure (Si-doped NFS-like hematite) decorated with IrO_2 nanoparticles [23] for PEC water splitting.

3.1. Synthesis of the Si-doped NFS-like hematite with IrO_2 surface decoration

Similarly to titanium, iron (Fe) has a relatively high melting temperature of $\sim 1550^\circ\text{C}$ under air condition and thus hematite nanostructures growth by simple thermal CVD or PVD using solid-phase Fe-compound precursors remains difficult. Instead, solution-phase precursors, such as $\text{Fe}(\text{CO})_5$, $\text{Fe}(\text{AcAc})_3$ and FeCl_3 , are used to provide sufficient amount of Fe precursors in the growth phase for the synthesis of hematite nanostructures via atmospheric pressure chemical vapor deposition (APCVD) or hydrothermal growth methods [23, 14, 16, 10].

However, the undoped hematite nanostructure is inactive or very inefficient when used as a photoanode for PEC water splitting, because of its low conductivity and improper conduction band position for hydrogen generation. To improve the conductivity, hematite has been doped by different elements, such as Si, Ti, Sn, Al, Mg and Zn, leading to increase the electron density. To address the issue of improper conduction band position of hematite, hematite surface decoration treatments with co-catalysts nanoparticles, such as IrO_2 nanoparticles [18], were applied to increase the chemical reactions of water oxidation.

As reported by Tilley et al. [23], Si-doped NFS-like hematite sample coated with IrO_2 nanoparticles was fabricated and a large photocurrent density of $\sim 3\text{ mA/cm}^2$ was obtained at a bias of $1.23\text{ V}_{\text{RHE}}$ under AM 1.5 illumination condition. In their synthesis process, a FTO-coated glass was used as the substrate for the NFS growth and put on an aluminum block heater. The substrate was maintained at 415°C during the APCVD growth process. The precursors $\text{Fe}(\text{CO})_5$ and tetraethoxysilane (TEOS) were carried to the FTO coated glass substrate by bubbling argon gas at fixed flow rates, calculated to be 3.5 mg/min for $\text{Fe}(\text{CO})_5$ and 0.32 mg/min for TEOS. These two streams were mixed with an air flow of 2 L/min and vertically sprayed to the substrate. After 5 minutes, NFS-like Si-doped hematite was synthesized. According to Tilley's reports, the preparation of homogeneous films on large substrates required a continuously rotating substrate in a rotating belt APCVD reactor. Moreover, the improved PEC performance with Si-doped NFS-like hematite photoanode needed a first growth of an ultrathin SiO_2 interfacial layer of $\sim 1\text{ nm}$ between hematite and FTO. It is very likely that this silica layer worked as an insulator layer to prevent the current leaking from the FTO layer to the electrolyte during the PEC experiments. Finally, the fabricated Si-doped NFS-like hematite was coated with $\sim 2\text{ nm}$ IrO_2 nanoparticles using an electrophoresis deposition process. An increased photocurrent of $\sim 3\text{ mA/cm}^2$ was achieved with the IrO_2 nanoparticles coating, to be compared with a photocurrent of $\sim 2\text{ mA/cm}^2$ obtained for the Si-doped NFS-like hematite without co-catalysts [23].

3.2. Characterization of the Si-doped NFS-like hematite with IrO₂ decoration

The cross-sectional SEM images of the synthesized Si-doped NFS-like hematite are shown in Fig. 3 a and 3b [23]. The hematite nanowires with an average height of ~ 500 nm were densely packed on the FTO-coated glass substrate. The diameter of the hematite nanowires at the top area varied from 75 to 250 nm. It is observed that the surfaces of hematite nanowires were very rough and composed of nanoparticles with diameters as small as ~ 10-20 nm. As suggested by Tilley et al., the rough surfaces further increased the nanowire/electrolyte interface areas and also shortened the diffusion length of the photogenerated holes to the interface areas, contributing to the increase of PEC water splitting performance [23].

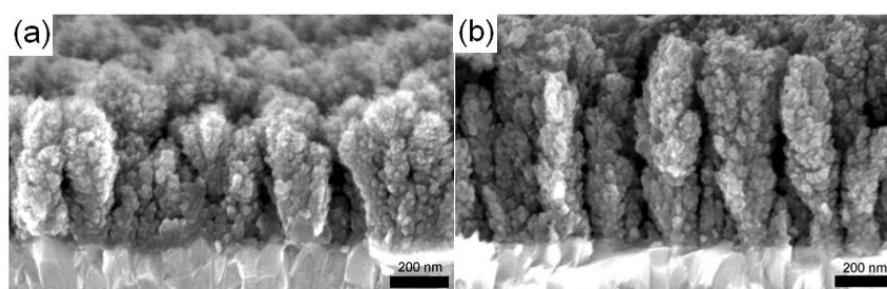


Figure 3. Cross-sectional SEM images of the dense and rough Si-doped NSF-like hematite. [23] Copyright John Wiley and Sons.

The microstructure and crystal quality of the NFS-like hematite samples with/without Si doping were further studied by XRD 2theta-omega scan technique. The XRD results are shown in Fig. 4. [13]. The undoped and Si-doped NFS-like hematite samples did not contain any other iron oxide phases than hematite, indicating a good experimental control over the hematite synthesis. The fact that the synthesized nanostructures are made of a single-phase hematite is important for the PEC water splitting applications, because other iron oxide phases such as Fe₃O₄ always contain strong electron-hole recombination centers, thus leading to lifetime degradation of the holes used in the oxidation of water [13]. Another important feature shown in the XRD results is that the crystal orientation of the synthesized hematite varied with the synthesis conditions. In the case of the undoped NSF-like hematite sample, there is no dominant crystal orientation. The intensities of the different X-ray diffraction peaks obtained with the undoped NSF-like hematite sample (see Fig. 4b) are similar to the XRD reference data measured on the randomly oriented hematite powders (see Fig. 4c). In contrast, the Si-doped NFS-like hematite sample showed a clear preferential [110] crystal orientation. These [110] oriented hematite nanowires likely have an enhanced conductivity compared to the randomly oriented hematite nanowires. In fact, the conductivity along the hematite [110] orientation was calculated to be of roughly four orders of magnitude higher than the conductivity along the other crystal orientations perpendicular to the [110] in hematite [12]. Therefore, the Si-doped NFS-like hematite with a preferential [110] orientation reported by Tilley et al. achieved a benchmark high photocurrent for PEC water splitting.

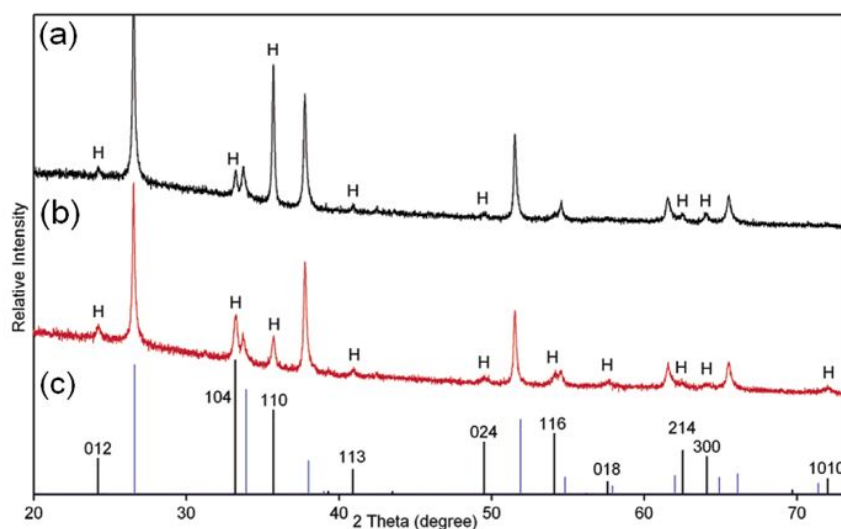


Figure 4. X-ray diffraction pattern of (a) Si-doped NFS-like hematite, (b) undoped NFS-like hematite, (c) standard powders of the hematite (black lines) and the SnO₂ (blue lines). Reprinted with permission from [13]. Copyright © 2006, American Chemical Society.

Finally, the synthesized Si-doped NFS-like hematite was coated with IrO₂ nanoparticles (~2 nm in diameter) by the electrophoresis deposition process [23]. The X-ray photoelectron spectroscopy (XPS) results showed an iridium concentration of ~1% on the surface of the IrO₂ coated sample, confirming the presence of IrO₂ [23].

3.3. PEC performance of the Si-doped NFS-like Hematite with IrO₂ decoration

The PEC performance of the IrO₂ decorated Si-doped NFS-like hematite was studied using a three-electrode PEC cell [23]. In the reported experiment, the Si-doped NFS-like hematite sample was used as the working electrode, an Ag/AgCl in a saturated KCl solution electrode was used as the reference electrode and a platinum wire was used as the counter electrode. One mole/liter NaOH solution with pH = 13.6 was used as the electrolyte. The sample was irradiated with the standard AM1.5 G 100 mW/cm² solar simulator.

The chrono-amperometry measurement of the hematite photoanode at a bias of 1.23 V_{RHE} with light on-off cycles shows that an on-off current behavior corresponding to the light on-off cycles is clearly observed (Fig. 5). The low dark current revealed that no/few chemical reactions occurred on the hematite photoanode without light illumination. A high photocurrent density of ~3 mA/cm² was obtained at a bias of 1.23 V_{RHE}, as shown in Fig. 5. This photocurrent decreased within the 200-second chrono-amperometry scan. As suggested by Tilley et al., the photocurrent decrease was related to the detachment of the IrO₂ nanoparticles from the surfaces of the Si-doped NFS-like hematite due to a weak chemical bonding between the IrO₂ and the hematite. More robust method to attach the IrO₂ nanoparticles on hematite should further improve the PEC results, as was suggested by Tilley et al. [23]

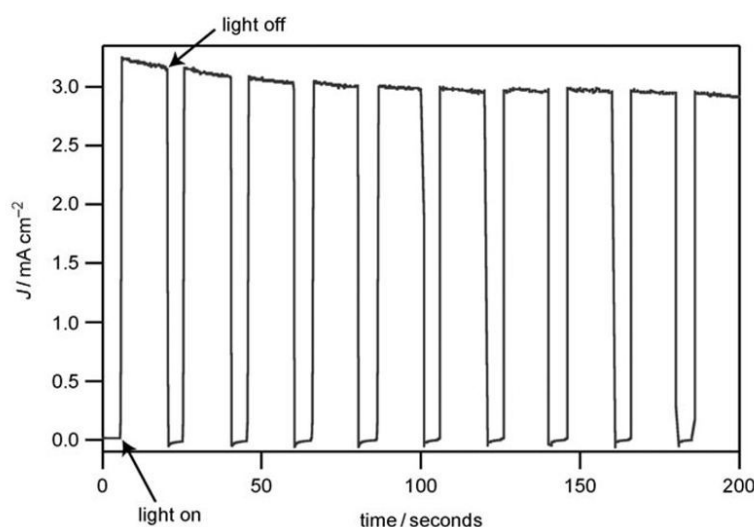


Figure 5. Chrono-amperometry measurements of the IrO₂ decorated Si-doped NFS-like hematite photoanode at a bias of 1.23 V_{RHE} under AM 1.5 G 100 mW/cm² light illumination [23] Copyright, John Wiley and Sons.

4. ZnO NFS for PEC water splitting

Due to their unique optoelectronic and semiconducting properties, single crystal ZnO densely packed nanowire arrays have been intensively studied in the past few decades for their potential use in electronic, electromechanical, and photonic devices [29, 20, 5, 26, 4, 32]. Recently, much research effort has been devoted to the fabrication of a high quality ZnO nanowire arrays and their application in PEC water splitting with the aim of taking advantage of ZnO material properties such as:

1. suitable band edge positions for PEC water splitting and
2. an increased conductivity when compared to TiO₂ and hematite for efficient charge transport [14, 30, 32].

For PEC water splitting applications, an efficient means permitting a good electrical connection of the nanowires through a conductive film, namely a ZnO NFS, is required. Yang et al. presented a detailed study on the fabrication and PEC performance of ZnO NFS (ZnO nanowire arrays on ITO film) with nitrogen doping [30]. An increased PEC photocurrent was obtained with the nitrogen-doped ZnO NFS sample. Wang et al. reported advanced PEC performances with CdS and CdSe quantum dots loaded ZnO NFSs under the conditions of sacrificial reagents [24]. However promising these results may be, further efforts to increase the stability of the ZnO NFSs in water under light illumination are required.

Since ZnO is chemically unstable in water under light irradiation, surface coating of the ZnO NFS with anti-photocorrosive and photocatalytic shell layers is one of the strategies to improve its chemical stability. However, the search for suitable anti-photocorrosive photocatalysts, which can grow easily on the ZnO nanowire surfaces with a high crystal quality, is a

major concern. One possible candidate for the shell material is ZnGa_2O_4 . Indeed, ZnGa_2O_4 is conductive, has anti-photocorrosive ability in water and photocatalytic property for PEC water splitting [11]. In addition, single crystal quality ZnGa_2O_4 can be synthesized via high-temperature chemical reactions using ZnO as the precursor material. Thus, surface coating of the ZnO NFS with conductive and anti-photocorrosive ZnGa_2O_4 shells to form ZnO- ZnGa_2O_4 core-shell NFS has been investigated [33]. With this structure, stable and efficient water splitting was achieved [32]. Further improvements are expected, including enhanced visible light absorption with doping, and efficient charge transfer to the electrolyte with the co-catalyst decoration of the ZnO nanowires.

In this section, we first review the synthesis of high crystal quality ZnO NFSs using different approaches. The realization of high quality ZnO nanowire arrays with efficient electrical connection is crucial for their subsequent use in high performance PEC cells. Then, the surface coating of the anti-photocorrosive ZnGa_2O_4 shells on the ZnO NFS is presented. Finally, the electronic properties and a stable PEC performance of the single crystal ZnO- ZnGa_2O_4 core-shell NFS are reported in detail.

4.1. Synthesis of the ZnO NFSs

A variety of physical and chemical approaches have been used to synthesize dense and single crystal ZnO nanowire arrays, including laser interference lithography [27], template-assisted wet-chemical growth [30, 4], MOCVD [21] and CVD [29, 5, 34]. As evidenced by these reports, the choice of a suitable substrate is of highest importance to synthesize single crystal ZnO nanowires with an aligned geometry.

Sapphire is a chemically stable and relatively cheap ceramic material and thus has been widely used as substrates for the growth of ZnO nanowire arrays in various fabrication processes. Erdélyi, et al. reported the synthesis of a single crystal quality and mono-oriented ZnO nanowire array on a *c*-plane sapphire by the pulsed laser deposition [4]. In their experiment, the pre-growth of a high quality and size controlled ZnO nanoseeds is needed for the growth of the nanowires. The top-view SEM image of the ZnO nanowire array is shown in Fig. 6 a. Because sapphire is an insulator, the as-grown ZnO nanowires on the sapphire substrate are not electrically connected, preventing their efficient use in optoelectronic applications. Thus, high quality ZnO nanowire arrays grown on conductive films are a prerequisite to the development of advanced nanowire-based materials.

One strategy is to form ZnO NFS on metal substrates. However, the growth of nanowires on metal substrate presents many difficulties. Three major issues should be addressed to realize the functionality of the ZnO NFS using metal substrates. They are as follows:

1. In order to avoid the formation of a Schottky barrier at the interfaces between the ZnO nanowires and the metal substrate, the work function of the metal should be lower than the Fermi level of the ZnO. This requirement severely limits the possible candidates for the metal substrates.
2. Metal substrates usually have large lattice mismatches with ZnO and, therefore, a pre-growth of lattice matched ZnO nanoseeds on the metal substrate is necessary to obtain

vertically aligned ZnO nanowires. As a result, the fabrication process becomes intricate, hard to control and expensive.

3. Another difficult issue related to the metal/ZnO interface is the existence of interface defects between the ZnO nanowires and the metal substrates, or even the formation of an insulator metal oxides layer at the nanowire and substrate interface that will block electron transport.
4. Finally for the purpose of PEC applications, an insulator layer should be deposited over the metal substrate surfaces that are not covered by nanowires in order to prevent a short circuit between the metal substrate and the electrolyte when this structure is used as photoanode.

In summary, the ZnO nanowire array on a metal substrate is still difficult to fabricate with adequate functionalities for use as a photoanode in a PEC cell.

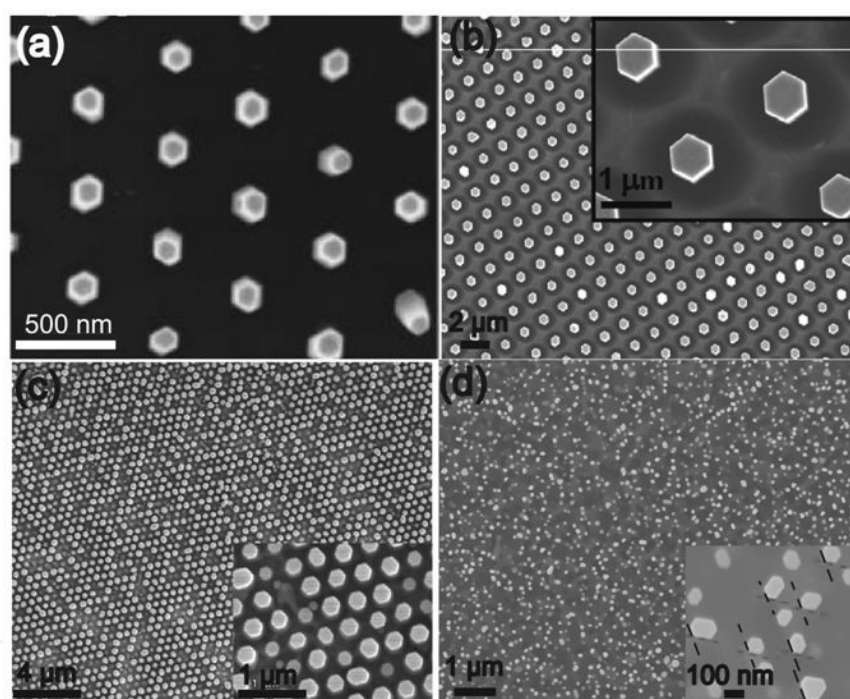


Figure 6. Top-view SEM images of vertically aligned ZnO nanowires on the (a) *c*-plane sapphire. Reprinted with permission from [4]. Copyright © 2011, American Chemical Society. (b) GaN substrate. Reprinted with permission from [27]. Copyright © 2010, American Chemical Society. (c) GaN substrate. [27] Copyright, John Wiley and Sons. (d) high quality ZnO film using *a*-plane sapphire as substrate. [34]

A different strategy is to grow ZnO nanowire arrays on conductive semiconductor substrates. GaN matches the in-plane geometry and lattice constants with ZnO and, therefore, has been employed as a high-quality epitaxial substrate for the growth of ZnO nanowire arrays [5, 27]. Fan et al. and Wei et al. synthesized orderly aligned, size-controlled and single crystalline quality ZnO nanowire arrays using single crystal GaN as substrates via a template-assisted growth process. In Fan's method, a porous anodic alumina membrane was

used as a template mask to control the gold catalysts deposition on the GaN substrate, whereas in Wei's method, laser interference lithography technique was used for a pre-growth of high quality ZnO nanoseeds on the GaN substrate. According to their reports, the diameters and distributions of the synthesized ZnO nanowires are governed by the parameters of the porous alumina membrane and the laser interference lithography techniques, respectively. The top-view SEM images of the synthesized ZnO nanowires are shown in Fig 6 b and 6c. Advanced piezo-electric performances have been reported for the fabricated ZnO NFSs. For the use in PEC applications, special attention should be paid to the interface defects and the barrier formation between the ZnO and the GaN in order to realize an efficient electrical charge collection.

The fabrication of a high quality ZnO nanowire array on a ZnO film (ZnO NFS) using a single-step CVD process has been recently reported by our group [34]. The synthesis process enables the growth of a dense ZnO nanowires array on a ZnO film. The nanowires, as well as the film, have a single crystal domain texture quality and the nanowires are perfectly aligned over a large area, which comes as the result of the single crystal domain texture. The top-view SEM image of the fabricated array is shown in Fig 6 d. Efficient electrical connection is realized because nanowires and the underneath film layer are made of the same material ZnO [34]. Compared to other growth processes of ZnO NFSs, our one-step CVD process is easily controlled and cheap. However, the diameters and distributions of the ZnO nanowires cannot be as precisely controlled as in the template-assisted growth processes. The synthesized ZnO NFS offers an ideal template for the subsequent synthesis of a single crystal ZnO-ZnGa₂O₄ core-shell NFS, which provides anti-photocorrosive property for the PEC applications.

4.2. Synthesis of the ZnO-ZnGa₂O₄ core-shell NFSs

ZnGa₂O₄ is a ternary metal oxide compound with a complicated crystal structure: one conventional ZnGa₂O₄ unit cell is composed of 8 Zn atoms, 16 Ga atoms and 32 O atoms, arranged into a spinel structure [6]. The direct fabrication of ZnGa₂O₄ nanowire array with a single crystal quality is very difficult and has not been reported yet. Thus, a two-step process to grow dense ZnO-ZnGa₂O₄ core-shell NFS has been proposed recently [33]:

1. synthesis of the high quality ZnO NFS and
2. surface coating of the ZnO NFS with the ZnGa₂O₄ shells (Fig. 7).

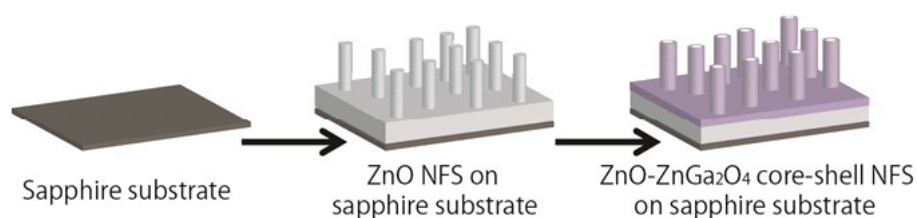


Figure 7. Schematic illustration of the fabrication process of the ZnO-ZnGa₂O₄ core-shell NFS. [32]

A high quality ZnO NFS consisting of dense and vertically aligned nanowires on the ZnO film was first fabricated using an *a*-plane sapphire substrate through a simple thermal CVD process [32]. In this process, Au-coated *a*-plane sapphire was selected as the growth substrate. ZnO powder and graphite powder mixed with a 2:1 weight ratio were used as source material and placed at 1 cm upstream position away from the substrate in a tubular furnace. The furnace was operated at 1000 °C for 30 minutes with the argon and oxygen gas mixture (5:1 in volume ratio) flowing through the tube at the working pressure of 50 mbar. At the end of the synthesis, the furnace cooled down naturally to the room temperature. The synthesized product consisted of a dense nanowires array on a ZnO film (ZnO NFS). Such a structure offers several advantages, namely,

1. the ZnO nanowires grown on the ZnO film are less prone to the formation of defects at the interface between the nanowires and the film and thus an efficient electrical connection of the ZnO nanowires is realized;
2. the underneath ZnO film is stable at high temperature, which enables the subsequent growth of the ZnGa₂O₄ shells in the second CVD step, without damaging the NFS.

In a second step, a CVD growth was performed on the ZnO NFS sample. The sample was put in a furnace at a temperature of 900°C. Mixed precursors of Ga₂O₃, ZnO and graphite were placed at 11 cm upstream position from the sample. The temperature of the precursor zone was set to 1180 °C. The carrier gases consisted of the argon and oxygen (10:1 in volume ratio) at the working pressure of 50 mbar. After a 30 minutes-long growth, the ZnO-ZnGa₂O₄ core-shell NFS was obtained [32].

4.3. Characterization of ZnO-ZnGa₂O₄ core-shell NFSs

The morphologies of the synthesized ZnO and ZnO-ZnGa₂O₄ core-shell NFSs are presented in Fig. 8. The tilted-angle SEM image of Fig. 8a shows a highly uniform and densely ZnO nanowire array grown over a large area on the Au-coated *a*-plane sapphire substrate. The inset in Fig. 8a is an enlarged SEM image revealing the vertically aligned nanowires. The vertical alignment and smooth sidewalls of the nanowires can be clearly observed. The average diameter of the nanowires is ~70 nm and the average length is about 1 μm. Energy-dispersive X-ray analyses (EDX) performed on the nanowire array gave a Zn/O atomic ratio of ~1/1, indicating the formation of the ZnO nanowires [34].

The tilted-angle SEM image of Fig. 8b shows a densely packed array of ZnO-ZnGa₂O₄ core-shell nanowires homogeneously arranged over large areas. The inset in Fig. 8b is an enlarged SEM image of the vertically aligned ZnO-ZnGa₂O₄ core-shell nanowires. The initial vertical alignment of the ZnO nanowires is well maintained in the ZnO-ZnGa₂O₄ core-shell nanowire sample. The average diameter of the ZnO-ZnGa₂O₄ core-shell nanowires is ~100 nm. EDX analysis performed on the surfaces of the core-shell nanowire gave a Zn/Ga/O atomic ratio of ~14/28/58 (~1/2/4), indicating the formation of the ZnGa₂O₄ shells. [32] In this work, a nanowires-on-a-film structure

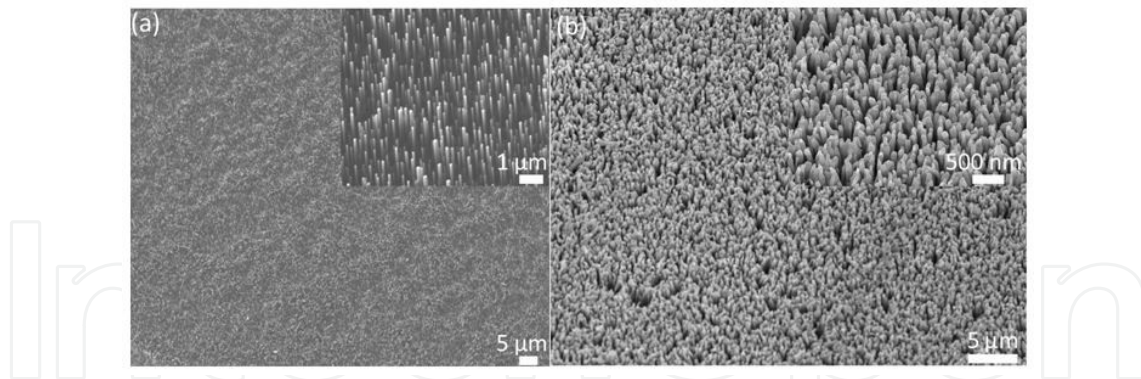


Figure 8. Tilted-angle SEM image of the dense and vertically aligned (a) ZnO and (b) ZnO-ZnGa₂O₄ nanowire arrays on the *a*-plane sapphire substrate. Insets in (a) and (b) are close-up images of the vertically aligned ZnO and ZnO-ZnGa₂O₄ nanowires. [32 and 34]

TEM and electron diffraction (ED) were used to analyze the structure and the crystalline quality of the ZnO and ZnO-ZnGa₂O₄ core-shell NFSs. The cross-sectional high-angle annular dark-field (HAADF) TEM image of the ZnO NFS is shown in Fig. 9a (left image). The average length of the nanowires is about 1 μm and the thickness of the film is about 2.5 μm. Such a thick ZnO bottom layer realized the electrical connection of the nanowire array. The energy dispersive spectroscopy (EDS) mapping images presented in Fig. 9a (the central image) clearly reveal that the NFS is made of ZnO and fabricated on the *a*-plane sapphire substrate.

ED analyses were further performed to characterize the crystal quality and the crystallographic orientation of the ZnO NFS sample. The ED pattern with the incident zone axis of [1-100] (see the right image in Fig. 9a) shows that the ZnO nanowire array and ZnO thick film are all single crystalline and well-aligned along the wurtzite [0001] direction. Such a single crystal and unique [0001] oriented ZnO NFS offers an ideal substrate for the subsequent growth of the ZnO-ZnGa₂O₄ core-shell NFS.

The TEM and ED results of the ZnO-ZnGa₂O₄ core-shell NFS are shown in Fig. 9b [33]. The bright-field TEM image reveals the nanowire core-shell structure with a different brightness contrast. The ED pattern of the shell region marked as the square A in the fig. 9b presented in the inset A of this figure shows that the shell part of the nanowire consists of a single-crystalline spinel ZnGa₂O₄ with a [111] direction parallel to the long axial direction of the nanowire. The ED pattern of the core region of B (square B, the ED pattern is shown in the inset B) confirms that the core part of the nanowire is a single crystal wurtzite ZnO with a [0002] direction parallel to the long axial direction of the nanowire. Furthermore, the ED pattern taken on the interfacial region of C (square C, the ED pattern is shown in the inset C) clearly shows two sets of single-crystalline electron diffraction dot patterns, indexed to the spinel ZnGa₂O₄ and the wurtzite ZnO. From the electron diffraction pattern, it is found that the ZnGa₂O₄ [111] direction is parallel to the ZnO [0002] direction and the ZnGa₂O₄ [2-20] direction is parallel to the ZnO [-2110] direction. An epitaxial relationship between the ZnGa₂O₄ (11-2) plane and the ZnO (1-100) plane is therefore predicted. Thus the subsequent growth of ZnGa₂O₄ on the ZnO NFS results in a hetero-epitaxial growth of the ZnGa₂O₄ shells on the ZnO cores. The final product is well-aligned ZnO-ZnGa₂O₄ core-shell nanowires.

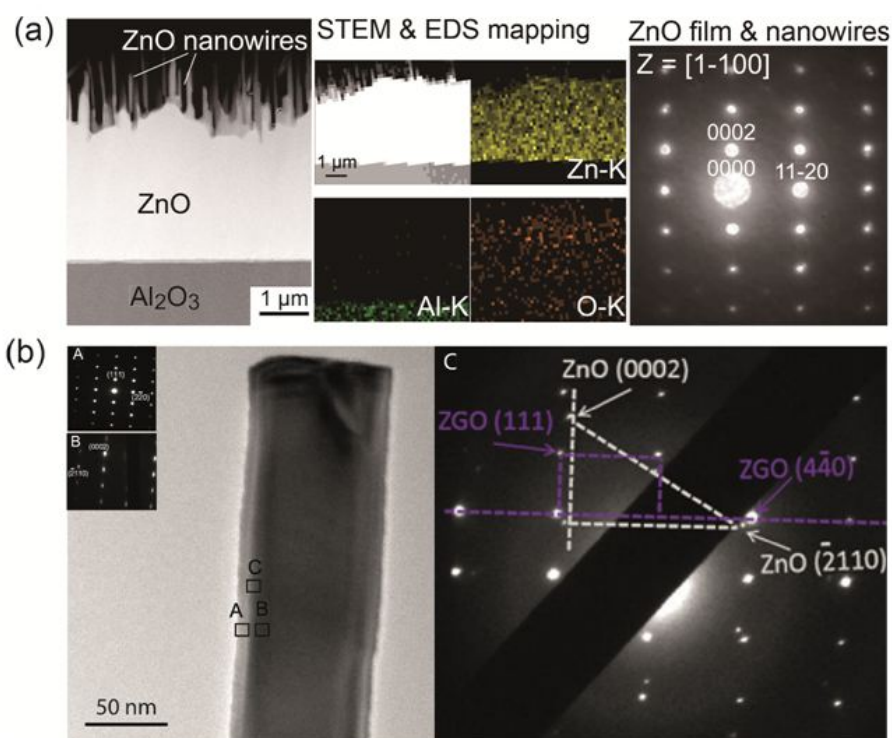


Figure 9. TEM, EDX-mapping and ED analyses of the dense and vertically aligned (a) ZnO and (b) ZnO-ZnGa₂O₄ nanowire arrays. [33 and 34]

Finally, standard X-ray diffraction (XRD) 2θ - ω scans were performed to examine the crystal structure and crystal orientations of the ZnO NFS and ZnO-ZnGa₂O₄ core-shell NFS over large areas [32 and 34]. Only two main diffraction peaks indexed to the wurtzite ZnO (0002) and (0004) planes were observed on the ZnO NFS sample, indicating a unique out-of-plane crystallographic orientation of the synthesized ZnO NFS over large areas. Furthermore, Zhong et al. performed XRD pole figure and rocking curve measurements. A single crystal domain texture quality (a unique in-plane and out-of-plane orientation over large areas) of the synthesized ZnO NFS was concluded. Such a high quality ZnO NFS was synthesized thanks to a new epitaxial process involving two growth steps. An epitaxial synthesis of the (0001) ZnO on the (11-20) sapphire substrate likely occurred at the beginning of the growth, helping to lock the in-plane orientation of the (0001) ZnO crystal. The Zn atoms then diffused into the Al₂O₃ substrate to form a single crystal, resulting into an intermediate layer of [0-21] oriented ZnAl₂O₄. This layer provides an improved in-plane geometry and lattice constant matching over the *a* plane of sapphire and, therefore, helps sustaining the growth of the high quality (0001) ZnO [34]. The fabricated high quality ZnO NFS can be seen as an ideal template to support the synthesis of a single crystal quality ZnO-ZnGa₂O₄ core-shell NFS. The XRD 2θ - ω scan result of the core-shell NFS shows only four diffraction peaks. Two diffraction peaks are indexed to the wurtzite ZnO (0002) and (0004) of the cores, and the other two diffraction peaks are indexed to the spinel ZnGa₂O₄ (111) and (222) of the shells. This result is strong evidence that the ZnO cores and ZnGa₂O₄ shells were both of a single crystal

quality and that the crystallographic axes of [0001] ZnO and [111] ZnGa₂O₄ are well aligned over large areas.

4.4. Electronic properties of ZnO-ZnGa₂O₄ core-shell NFSs

It is of first importance for the development of PEC water splitting cells to understand the electronic properties of the ZnO-ZnGa₂O₄ core-shell NFS photoanode in the electrolyte solution. The carrier density and the flatband potential of the ZnO-ZnGa₂O₄ core-shell NFS were measured by electrochemical impedance spectroscopy [32]. For this purpose, a solution of 0.5 M NaClO₄ buffered (pH of 7.0) was used as an electrolyte, Ag/AgCl electrode in saturated KCl solution as the reference electrode, a Pt wire as the counter electrode and the ZnO-ZnGa₂O₄ core-shell NFS sample as a working electrode. Prior to the electrochemical impedance measurement, N₂ gas was bubbled for 10 minutes to get rid of O₂ in the electrolyte solution. The electrochemical impedance analysis was then performed for a bias ranging from -1 to 1 V (versus Ag/AgCl), at the frequency of 1 kHz under dark condition. The results of this experiment are presented in a $1/C^2$ vs. V plot (Fig. 10a).

The carrier density and the flatband potential of the cylindrical nanowires were quantified using the model proposed by [17]. Solving the Poisson equation with a cylindrical capacitance approximation at the nanowire/electrolyte interfaces, we obtain:

$$\frac{1}{r} \frac{\partial}{\partial r} \left(r \frac{\partial V}{\partial r} \right) = - \frac{q}{\epsilon \epsilon_0} N_d \quad (1)$$

$$C_s = \frac{2\epsilon \epsilon_0 x^2}{R(R^2 - x^2)} \quad (2)$$

where R is the radius of the nanowires, x the central radius of the quasi-neutral region in the nanowires, C_s the capacitance per unit area of the nanowires, V the applied bias between the electrodes, V_{FB} the flatband potential of the nanowire at the nanowire/electrolyte interface, q the unit electron charge, ϵ_0 the permittivity of vacuum and ϵ the relative dielectric constant of ZnO. The results of the fitting of the measured $1/C^2$ vs. V curve according to the Mora-Seró model are shown in Fig. 10 b. The carrier density of the ZnO-ZnGa₂O₄ nanowires was estimated to be $\sim 10^{19}$ cm⁻³. According to the literature [1, 28, 34], the carrier density of the undoped ZnO nanowires is usually around $\sim 10^{17} - 10^{18}$ cm⁻³. The increase in the carrier density of the ZnO-ZnGa₂O₄ NFS sample compared to that of the ZnO nanowires can be understood as the formation of conductive ZnGa₂O₄ shell layers and the introduction of Ga donors inside the ZnO cores [19, 31]. The increased carrier density in the ZnO-ZnGa₂O₄ nanowires decreases their electrical resistance and thus contributes to a reduced energy loss for PEC water splitting applications.

The flatband potential of the ZnO-ZnGa₂O₄ NFS sample at the nanowire/electrolyte interface is another important parameter when analyzing the photoanodes properties for water

splitting in a PEC cell. Typically, a negative flatband potential and an upward band bending occur at the interface between an *n*-type semiconductor and an electrolyte, due to their Fermi-level difference [22]. A schematic illustration of the band bending with a contact energy barrier at an idealized interface between a *n*-type semiconductor in equilibrium with an electrolyte is shown in Fig. 10 c. The flat-band potential of the ZnO-ZnGa₂O₄ core-shell NFS sample was estimated to be about -0.4 V (versus NHE). The cathodic flatband potential of the ZnO-ZnGa₂O₄ NFS sample provides a suitable energy band position for PEC water splitting.

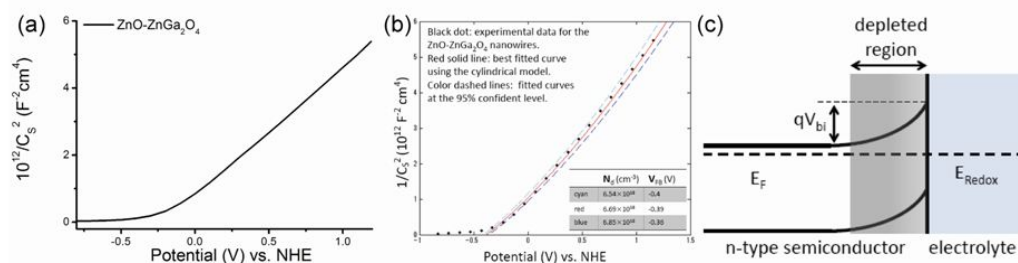


Figure 10. a) Electrochemical impedance plot of the ZnO-ZnGa₂O₄ NFS sample at the frequency of 1 kHz in dark condition with a bias varying from -0.8 to 1.2 V (versus NHE); (b) Fitted curves of ZnO-ZnGa₂O₄ NFS sample with an assumed ϵ value of 10 for the ZnO-ZnGa₂O₄ nanowires; (c) A schematic of the surface band bending at an idealized interface between an *n*-type semiconductor and an electrolyte in equilibrium. qV_{bi} is the energy barrier height at the interface. [32] - Reproduced by permission of The Royal Society of Chemistry.

4.5. PEC performances of ZnO-ZnGa₂O₄ core-shell NFSs

The PEC performance of the ZnO-ZnGa₂O₄ NFS sample used as a photoanode was studied in a 0.1 M Na₂SO₄ electrolyte solution at pH = 6 under illumination with a 300 W Xenon lamp [32]. An Ag/AgCl electrode in a saturated KCl solution was used as the reference electrode and a Pt wire used as the counter electrode. Fig. 11a shows the current-voltage curve for the ZnO-ZnGa₂O₄ nanowire array at a bias ranging from -0.8 V to 1 V (versus Ag/AgCl) with light on-off cycles, indicating a good photoresponsibility of the NFS sample used as photoanode. The flatband potential of the NFS sample is equivalent to the onset potential of the anodic photocurrent, as shown to be ~ -0.35 V vs. NHE with an estimated error of ± 0.1 V in the inset of Fig. 11a [32]. This value of the onset potential agreed well with the flatband potential of ~ -0.4 V estimated from the fit of the electrochemical impedance data in Fig. 10 b.

The amperometric study of the ZnO-ZnGa₂O₄ core-shell nanowire array was performed at a fixed bias of 1.23 V_{RHE} under on-off illumination cycles. The obtained data are plotted in the form of current-time curve (Fig. 11b). The result shows a very low current of $< 10^{-4}$ mA/cm² under dark conditions, indicating the absence of any chemical reaction at the ZnO-ZnGa₂O₄ NFS anode for an applied bias of 1.23 V_{RHE} under dark conditions. Under illumination, a large photocurrent with a steady value of 1.2 mA/cm² was obtained, indicating a stable and efficient photoelectrolysis of water at the surface of the ZnO-ZnGa₂O₄ NFS photoanode. As a comparison, the photocurrent measured on ZnO or *n*-doped ZnO nanowire array always deteriorates with time under continuous light illumination, confirming that ZnO is chemi-

cally unstable in water under illumination (Li et al. 2009). After switching off the light illuminating the ZnO-ZnGa₂O₄ NFS anode, a fast recovery of the current to the dark current value was clearly observed. The on-off current cycles presented a very good reproducibility and anti-photocorrosion stability as shown in Fig. 11 b. Therefore, the core-shell NFS demonstrated an improved stability and a large photocurrent of 1.2 mA/cm² when used as the photoanode in the PEC water splitting cell [32].

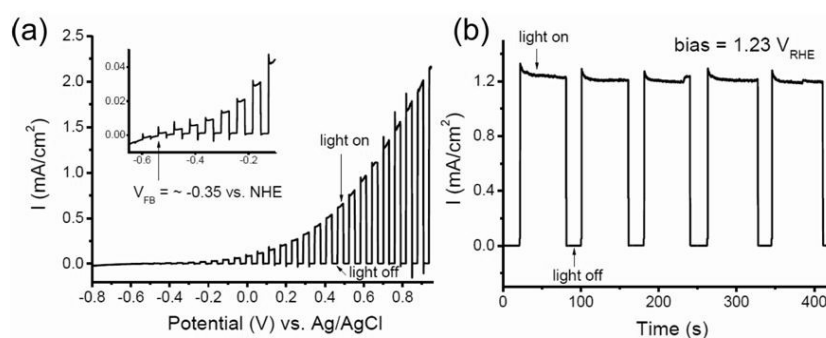


Figure 11. a) Current-voltage curves of the ZnO-ZnGa₂O₄ NFS sample in an electrolyte of 0.1 M Na₂SO₄ at pH = 6 under illumination with a 300 W Xenon lamp. Sweep rate of the voltage was 0.5 mV/s. (b) Current-time curve of the ZnO-ZnGa₂O₄ NFS when used as a photoanode at an applied bias of 1.23 V_{RHE} with light on-off cycles. [32] - Reproduced by permission of The Royal Society of Chemistry.

5. Conclusions

Recent advances in the development of densely packed and single crystalline quality semiconductor NFSs with a controllable doping level offer promising opportunities for the future PEC water splitting applications. In this type of nanostructured photoanodes, an improved light absorption, enhanced charge separation and an increased surface area for chemical reaction are obtained due to the shell layer of the semiconductor nanowire array of the NFS. Further, the film underneath the nanowires realizes an efficient electrical connection of the semiconductor nanowire array, thus facilitating the direct use of the NFS as the photoanode in PEC water splitting applications. However, many difficulties still remain to be resolved. Two essential issues related to the reliability and the efficiency needs to be addressed for all the PEC water splitting systems. In this Chapter, the NFS-based photoanodes made of different semiconductor photocatalysts have been reviewed and their advantages and the remaining challenges have been discussed in detail. The TiO₂ NFS photoanode has an excellent chemical stability in water, but its large bandgap and inefficient doping limit the efficiency in the PEC applications under solar illumination. The hematite NFS photoanodes have a bandgap which permits a good photoresponsivity under the illumination with the visible part of the solar spectrum and a good chemical stability in water. However, the large resistance and inadequate energy band position of the hematite render this NFS inefficient for the PEC applications without any further efficient doping and the co-catalysts dec-

oration. An efficient doping and the co-catalyst decoration of the hematite NFS have not yet been achieved to improve its performances and obtain a stable operation in water splitting PEC. The ZnO-ZnGa₂O₄ core-shell NFS photoanode offers an enhanced conductivity over TiO₂ and hematite, as well as anti-photocorrosive property in water. Thus this material offers stable and efficient operation of water splitting PEC. However, the ZnO-ZnGa₂O₄ core-shell NFS only responds to the UV light, which results in a low efficiency under solar light illumination. Further work is now in progress to achieve an efficient and stable solar water splitting with doped ZnO-ZnGa₂O₄ core-shell NFSs. Besides the photocatalyst materials already fabricated in the form of NFSs reviewed in this Chapter, it is worth noting that a large variety of alternative photocatalysts exist, which can permit to grow nanostructures for high efficiency PEC applications. Finally, still more progress is expected to be made to realize an efficient and stable solar water splitting system permitting to achieve a new, sustainable and environmentally friendly hydrogen production method, contributing to a better daily life of human beings in the near future.

Author details

Miao Zhong¹, Mario Kurniawan¹, Aleksandra Apostoluk^{2*}, Bertrand Vilquin² and Jean-Jacques Delaunay^{1*}

*Address all correspondence to: jean@mech.t.u-tokyo.ac.jp

¹ School of Engineering, The University of Tokyo, Japan

² INL, CNRS UMR-5270, Lyon University, France

References

- [1] Allen, M. W., Alkaisi, M. M., & Durbin, S. M. (2006). Metal Schottky diodes on Zn-polar and O-polar bulk ZnO. *Appl. Phys. Lett.*, 89, 103520.
- [2] Bak, T., Nowotny, J., Rekas, M., & Sorrell, C. C. (2002). Photo-electrochemical hydrogen generation from water using solar energy. Materials-related aspects. *Inter. J. Hydro. Energy.*, 27, 991-1022.
- [3] Chen, X., & Mao, S. S. (2007). Titanium dioxide nanomaterials: synthesis, properties, modifications, and applications. *Chem. Rev.*, 107, 2891-2959.
- [4] Erdélyi, R., Nagata, T., Rogers, D. J., Teherani, E. H., Horváth, Z. E., Lábadi, Z., Baji, Z., Wakayama, Y., & Volk, J. (2011). Investigations into the impact of the template layer on ZnO nanowire arrays made using low temperature wet chemical growth. *Cryst. Growth Des.*, 11, 2515-2519.

- [5] Fan, H. J., Lee, W., Hauschild, R., Alexe, M., Rhun, G. L., Scholz, R., Dadgar, A., Nielsch, K., Kalt, H., Krost, A., Zacharias, M., & Gösele, U. (2006). Template-assisted large-scale ordered arrays of ZnO pillars for optical and piezoelectric applications. *Small*, 2, 561-568.
- [6] Fan, H. J., Yang, Y., & Zacharias, M. (2009). ZnO-based ternary compound nanotubes and nanowires. *J. Mater. Chem.*, 19, 885-900.
- [7] Frank, S. N., & Bard, A. J. (1977). Heterogeneous photocatalytic oxidation of cyanide ion in aqueous solutions at titanium dioxide powder. *J. Am. Chem. Soc.*, 99, 303-304.
- [8] Feng, X., Shankar, K., Varghese, O. K., Paulose, M., Latempa, T. J., & Grimes, C. A. (2008). Vertically aligned single crystal TiO₂ nanowire arrays grown directly on transparent conducting oxide coated glass: synthesis details and applications. *Nano. Lett.*, 8, 3781-3786.
- [9] Fujishima, A., & Honda, K. (1972). Electrochemical photolysis of water at a semiconductor electrode. *Nature*, 283, 37-38.
- [10] Hoang, S., Guo, S., Hahn, N. T., Bard, A. J., & Mullins, C. B. (2011). Visible light driven photoelectrochemical water oxidation on nitrogen-modified TiO₂ nanowire. *Nano. Lett.*, 12, 26-32.
- [11] Ikarashi, K., Sato, J., Kobayashi, H., Saito, N., Nishiyama, H., & Inoue, Y. (2002). Photocatalysis of water decomposition by RuO₂-Dispersed ZnGa₂O₄ with d¹⁰ configuration. *J. Phys. Chem. B*, 106, 9048-9053.
- [12] Iordanova, N., Dupuis, M., & Rosso, K. M. (2005). Charge transport in metal oxides: A theoretical study of hematite α -FeO. *J. Chem. Phys.*, 122, 144305-1-10.
- [13] Kay, A., Cesar, I., & Grätzel, M. (2006). New benchmark for water photooxidation by nanostructured α -Fe₂O₃ films. *J. Am. Chem. Soc.*, 128, 15714-15721.
- [14] Krol, R. V. D., Liang, Y., & Schoonman, J. (2008). Solar hydrogen production with nanostructured metal oxide. *J. Mater. Chem.*, 18, 2311-2320.
- [15] Law, M., Greene, L. E., Johnson, J. C., Saykally, R., & Yang, P. (2005). Nanowire dye-sensitized solar cells. *Nature*, 4, 455-459.
- [16] Ling, Y., Wang, G., Wheeler, A. D., Zhang, J. Z., & Li, Y. (2011). Sn-doped hematite nanostructures for photoelectrochemical water splitting. *Nano. Lett.*, 11, 119-125.
- [17] Mora-Seró, I., Fabregat-Santiago, F., Denier, B., & Bisquert, J. (2006). Determination of carrier density of ZnO nanowires by electrochemical techniques. *Appl. Phys. Lett.*, 89, 203117-1-3.
- [18] Nakagawa, T., Beasley, C. A., & Murray, R. W. (2009). Efficient electro-oxidation of water near its reversible potential by a mesoporous IrO_x nanoparticle film. *J. Phys. Chem. C*, 113, 12958-12961.

- [19] Omata, T., Ueda, N., & Ueda, K. (1994). New ultraviolet-transport electroconductive oxide, ZnGa₂O₄ spinel. *Appl. Phys. Lett.*, 64, 1077-1078.
- [20] Özgür, Ü., Alivov, Ya. I., Liu, C., Teke, A., Reshchikov, M. A., Doğan, S., Avrutin, V., Cho, S. J., & Morkoç, H. (2005). A comprehensive review of ZnO. *Appl. Phys. Lett.*, 98, 041301-1-103.
- [21] Park, W. I., Kim, D. H., Jung, S. W., & Yi, G. (2002). Metalorganic vapor-phase epitaxial growth of vertically well-aligned ZnO nanorods. *Appl. Phys. Lett.*, 80, 4232-4234.
- [22] Sze, S. M., & Kwok, K. Ng. (2007). Physics of semiconductor devices. 3rd edition. Book, John Wiley & Sons.
- [23] Tilley, S. D., Cornuz, M., Sivula, K., & Grätzel, M. (2010). Light-induced water splitting with hematite: improved nanostructure and iridium oxide catalysis. *Angew. Chem. Int. Ed.*, 49, 6405-6408.
- [24] Wang, G., Yang, X., Qian, F., Zhang, J. Z., & Li, Y. (2010). Double-sided CdS and CdSe quantum dot co-sensitized ZnO nanowire arrays for photoelectrochemical hydrogen generation. 10, 1088-1092.
- [25] Wang, X., Song, J., Liu, J., & Wang, Z. L. (2007). Direct-Current Nanogenerator driven by ultrasonic waves. *Science*, 316, 102-105.
- [26] Wang, Z. L. (2009). Energy Harvesting Using Piezoelectric Nanowires-A Correspondence on "Energy Harvesting Using Nanowires?". by Alexe et al. *Adv. Mater.*, 21, 1311-1315.
- [27] Wei, Y., Wu, W., Guo, R., Yuan, D., Das, S., & Wang, Z. L. (2009). Wafer-scale high-throughput ordered growth of vertically aligned ZnO nanowire array. *Nano Lett.*, 10, 3414.
- [28] Wolcott, A., Smith, W. A., Kuykendall, T. R., Zhao, Y., & Zhang, J. Z. (2009). Photoelectrochemical study of nanostructured ZnO thin films for hydrogen generation from water splitting. *Adv. Funct. Mater.*, 19, 1849-1856.
- [29] Yang, P., Yan, H., Mao, S., Russo, R., Johnson, J., Saykally, R., Morris, N., Pham, J., He, R., & Choi, H. (2002). Controlled Growth of ZnO Nanowires and Their Optical Properties. *Adv. Funct. Mater.*, 12, 323.
- [30] Yang, X., Wolcott, A., Wang, G., Sobo, A., Fitzmorris, R. C., Qian, F., Zhang, J. Z., & Li, Y. (2009). Nitrogen-doped ZnO nanowire arrays for photoelectrochemical water splitting. *Nano Lett.*, 9, 2331.
- [31] Yuan, G., Zhang, W., Jie, J., Fan, X., Tang, J., Shafiq, I., Ye, Z., Lee, C., & Lee, S. (2008). Tunable n-Type Conductivity and Transport Properties of Ga-doped ZnO Nanowire Arrays. *Adv. Mater.*, 20, 168-173.
- [32] Zhong, M., Li, Y., Yamada, I., Delaunay, J., & J. (2012a). ZnO-ZnGa₂O₄ core-shell nanowire array for stable photoelectrochemical water splitting. *Nanoscale*, 77, 1509-1514.

- [33] Zhong, M., Li, Y., Tokizono, T., Zheng, M., Yamada, I., Delaunay, J., & , J. (2012b). Vertically aligned ZnO-ZnGa₂O₄ core-shell nanowires: from synthesis to optical properties. *J. Nanopart. Res.*, 14, 804-814.
- [34] Zhong, M., Sato, Y., Kurniawan, M., Apostoluk, A., Masenelli, B., Maeda, E., Ikuhara, Y., & Delaunay, J. J. (2012c). ZnO dense nanowire array on a film structure in a single crystal domain texture for optical and photoelectrochemical applications. *Nanotechnology*, accepted.

IntechOpen

IntechOpen